inorganic compounds

Synchrotron X-ray study of ortho-rhombic Rb₃Ta₅O₁₄ with a modified pyrochlore structure

Douglas du Boulay,* Reiko Yamashita† and Nobuo Ishizawa

Materials and Structures Laboratory, Tokyo Institute of Technology, 4259 Nagatsuta Midori, Yokohama 226-8503, Japan
Correspondence e-mail: ddb@r3401.rlem.titech.ac.jp

The structure of a new orthorhombic trirubidium pentatantalum oxide ($Rb_3Ta_5O_{14}$) phase with *Pnma* symmetry was identified from a half sphere of synchrotron X-ray data measured at a wavelength of 0.85 Å. This notionally linked TaO_6 octahedral structure broadly consists of three different modifications of the pyrochlore ring motif with layer stacking normal to (205) planes. Successive pyrochlore layers do not simply stack normal to these planes but are offset along the [100] axis. An unusual aspect of this structure is the occurrence of TaO_5 trigonal bipyramids in structurally complex regions where the modified pyrochlore rings connect.

Comment

The structure of the title RbTaO phase, shown in Fig. 1, contains four independent Rb atoms, seven independent Ta atoms, 17 independent O atoms and is comprised of three distinct Rb filled cavities (see Fig. 2a) delimited by predominantly corner-sharing TaO_6 octahedra. One of those cavities, having explicit $\bar{1}$ symmetry, is large enough to hold four Rb (2 × Rb3 and 2 × Rb4) atoms, while the other two exhibit explicit *m* symmetry, with pseudo-$\bar{1}$ symmetry, and contain only two Rb atoms (2 × Rb1 or 2 × Rb2). A diverse range of polyhedral linkages is exhibited by this structure: the $Ta1O_6$ and $Ta2O_6$ octahedra share one common edge; $Ta4O_6$ octahedra share a single edge with a $Ta6O_6$ octahedra; the $Ta6O_6$ octahedra edge shares with two $Ta4O_6$ octahedra and a $Ta5O_5$ trigonal bipyramid.

The structure reported here closely resembles that of the analogue material $Cs_3Ta_5O_{14}$ reported by Serafin & Hoppe (1982). Those authors report an orthorhombic unit cell [$a = 26.235$, $b = 7.429$ and $c = 7.388$ Å], with *Pbam* symmetry. Their structure has two distinct cavities, consisting of a large 4 × Cs filled cavity linked to four equivalent 2 × Cs filled cavities. In their analogue, both cavities have mirror symmetry, though for the larger cavity, it is explicitly 2/m. There is a very good

structural match between $Cs_3Ta_5O_{14}$ and $Rb_3Ta_5O_{14}$ if a pseudo-mirror plane present at $y = \frac{1}{2}$ in the latter structure becomes exact. This would halve the *b* axis giving close lattice-parameter agreement. It would also require the Rb3 and Rb4 atoms to sit exactly on a mirror plane and force the Rb1- and Rb2-filled cavities to adopt some common, intermediate, and presumably more regular geometry. In so doing, the Ta6-centred octahedra, which edge share with two other octahedra and the Ta5 trigonal-bipyramid, would have to deform further into a trigonal-bipyramid identical to, but still edge sharing with, that of Ta5. Ta1, Ta2, Ta3 and Ta4 already have decidedly asymmetric octahedral geometries, with five short and one long Ta—O bond, so a structural transition of the type just described for Ta6 is not unreasonable.
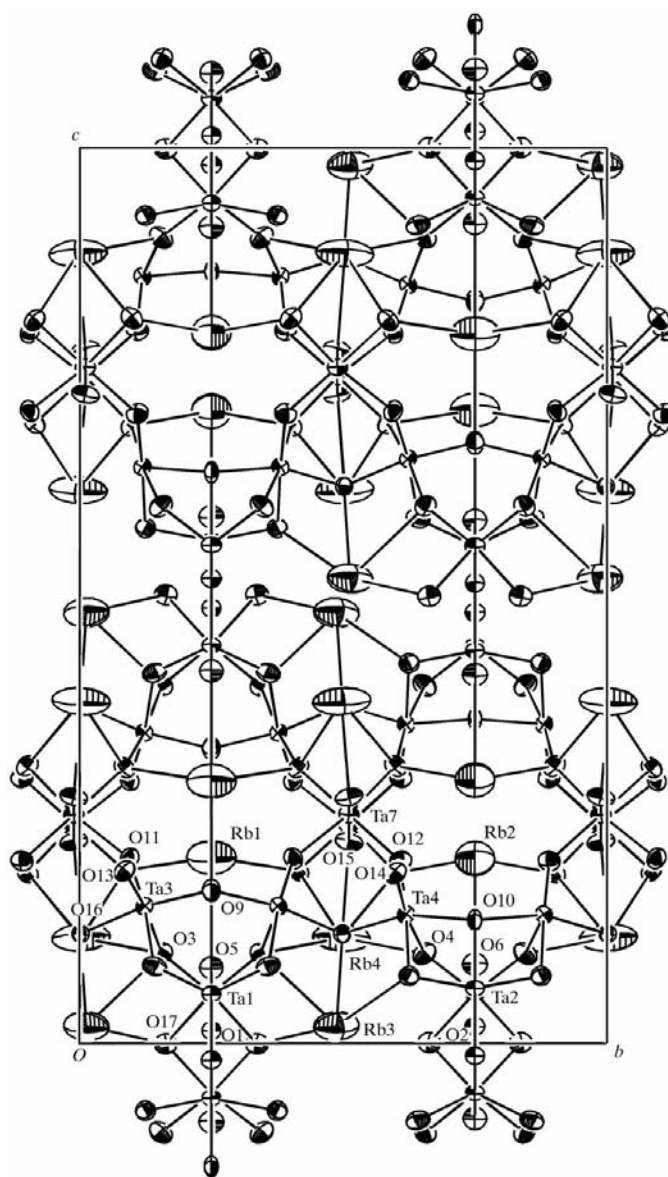

Figure 1
The mean-squared atomic displacements (*ORTEP*; Johnson, 1970), shown at the 90% probability level and projected down the *a* axis of $Rb_3Ta_5O_{14}$. Ta5 and Ta6 are occluded behind the Ta1 and Ta2 atoms, respectively.

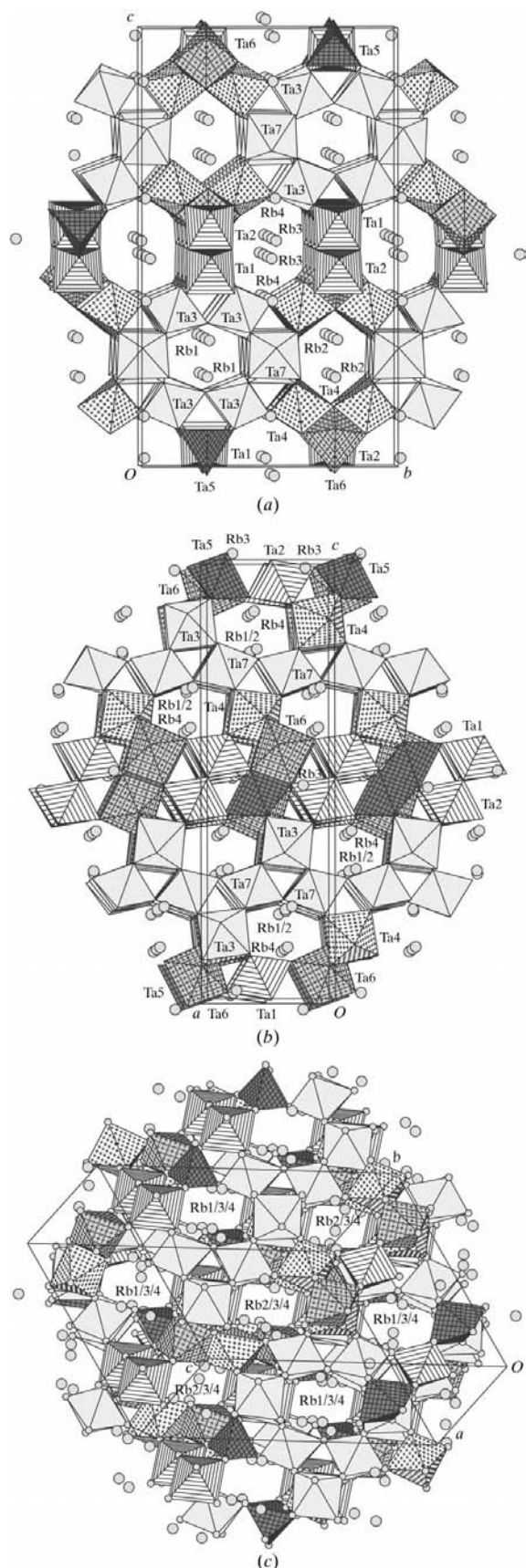† Present address: Toshiba Co., 1-9-2 Hatarachou, Hukaya, 366-8510, Japan.

Figure 2
Polyhedral (Dowty, 1995) sphere, 13 Å radius, centred on $(\frac{1}{2}, \frac{1}{2}, \frac{1}{2})$, showing (a) the [100] channels, (b) the [010] channels and (c) the [52$\bar{2}$] channels.

The $Cs_3Ta_5O_{14}$ structure reported by Serafin & Hoppe (1982) could be considered an archetype from which $Rb_3Ta_5O_{14}$ deviates. But, in fact, those authors reported a rather large agreement index [$R(F) = 0.10$] and refined their structure with isotropic Ta- and O-atom constraints. It is not inconceivable that those authors may have overlooked a very subtle deviation from their own archetype, towards that of $Rb_3Ta_5O_{14}$. It would have been apparent as very weak $l = n + \frac{1}{2}$ reflections corresponding to a doubling of their c axis.

To aid in classifying this material more completely, it is useful to relate its structure to polyhedral stacking sequences of related archetype structures. The hexagonal tungsten bronze (HTB) archetype (Kihlborg & Hussain, 1979) $K_{0.32}WO_3$ has $P6_3/mcm$ symmetry consisting of entirely corner-shared WO_6 octahedra arranged in linked coplanar six-membered rings, such that each octahedron is involved in two rings. This leads to hexagonal-shaped cavities containing K atoms and small triangular-shaped cavities where three six-membered rings pack. HTB has a one-layer repeat structure, with successive octahedral ring-system layers stacked, corner-sharing, in perfect alignment. In the $Cd_2Nb_2O_7$ pyrochlore (Lukaszewicz *et al.*, 1994) variation on HTB, additional tilting of the octahedra in the plane of the six-membered rings leads the triangular cavities to split into two separate classes, one small and one large alternating in sequence around each ring. The smaller cavities are actually capped by isolated NbO_6 octahedra on a second layer, with the pyrochlore ring structure repeated again in the third layer, *i.e.* it is a two-layer repeat structure.

Fig. 3 shows a (205) plane cross-section through the $Rb_3Ta_5O_{14}$ structure. It clearly shows three distinct variations of the pyrochlore ring system which extend in chains infinitely along the b axis. The next (205) plane layer (Fig. 4) illustrates a network of cavities and channels with isolated polyhedra delimiting the channel and cavity walls. These are analogues of the cavity-capping octahedra above the small triangular cavities around the true pyrochlore rings in the $Cd_2Nb_2O_7$ structure. Subsequent layers are simply repeats of these first two layers, but with an offset equal to one unit-cell translation along the a axis. This description suggests that $Rb_3Ta_5O_{14}$ has a two-layer repeat structure similar to pyrochlore, but in fact the small planar subsections illustrated in Figs. 3 and 4 co-exist in the same plane, alternating as chains of rings and channels running parallel to b. Strictly speaking then, $Rb_3Ta_5O_{14}$ is a single-layer structure, with large oscillatory offsets oriented such that the structure normal to those planes is never repeated with perfect alignment.

It can be seen in Fig. 3 that the large and very distorted eight-membered pyrochlore-like ring system has two pairs of nearly parallel edges comprised of pairs of edge-sharing ($Ta1O_6$ and $Ta2O_6$) octahedra. Those edge-sharing octahedra are corner linked to a trigonal bipyramid ($Ta5O_5$) and octahedra ($Ta6O_6$) that edge share in successive isolated layers. Unbroken chains of Ta1- and Ta2-centred octahedra, followed by $Ta5O_5$ and $Ta6O_6$ polyhedra repeat infinitely along the a axis and clearly delimit the walls of a long channel containing the Rb3 and Rb4 atoms, as shown in Fig. 2(a).

inorganic compounds

The two distinct six-membered pyrochlore-like ring systems are also shown in Fig. 3. One of these, containing the Rb1 atoms, is comprised entirely of corner-sharing octahedra and more closely resembles the pyrochlore archetype. The other pyrochlore-like ring, containing the Rb2 atoms, is comprised of two pairs of octahedra, each pair edge sharing to a common third octahedra, though only one is fully contained in the Fig. 3 planar subsection. This edge sharing deforms the pyrochlore ring structure to a greater extent than is seen for the Rb1 pyrochlore ring. A sequence of purely corner-sharing $Ta7O_6$ octahedra form continuous chains parallel to the a axis which appear in Fig. 2(a) as walls separating the Rb1- and Rb2-filled channels.

The pyrochlore-like layers, isolated layers and channels are all different aspects of a structure that could be described more collectively as a network of three complex, irregularly shaped, Rb-filled cavities with edges delimited by Ta–O polyhedra. Each has six large openings where the cavity faces intersect, typically hexagonal in shape but for the large $4 \times$ Rb filled cavities connected along the [100] axis, those channels resemble larger puckered octagonal faces.

All of the three independent cavities in $Rb_3Ta_5O_{14}$ interface with two cavities of the same type stacked along the short a axis (see Fig. 2a) and also with four cavities of an alternate size along the four approximate [0±1±1] vectors (actually [52$\bar{2}$] in Fig. 2c). Figs. 2(b) and 2(c) are images of the lattice oriented to highlight the continuous channels through the cavity [0±1±1] interfaces. 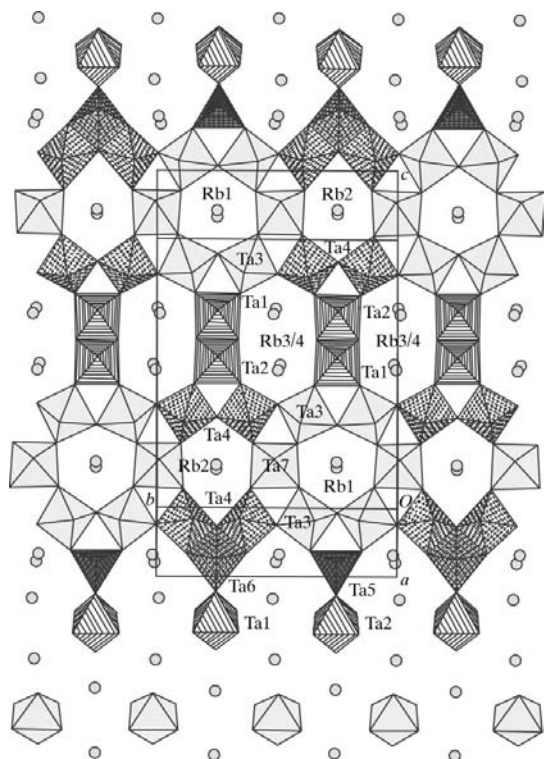The projection axes of these figures correspond broadly to uninterrupted horizontal and diagonal paths in the plane of the Fig. 4 isolated polyhedral layer. For Fig. 2(b), the planar cavity interfaces are oriented at around 30° to the image projection vector so the linear channels appear quite narrow. In this image, the channels intersect different cavities in the sequence $2 \times$ Rb1–$4 \times$ Rb(3,4)–$2 \times$ Rb2–$4 \times$ Rb(3,4). In Fig. 2(c), the $\simeq$ [0±1±1] cavity interfaces are normal to the viewing vector, but the off-centred alignment of consecutive interfaces reduces the apparent aperture of the channels. Here, the channels intersect the cavities in two distinct sequences i.e. $2 \times$ Rb1–$4 \times$ Rb(3,4)–$2 \times$ Rb1–$4 \times$ Rb(3,4) and $2 \times$ Rb2–$4 \times$ Rb(3,4)–$2 \times$ Rb2–$4 \times$ Rb(3,4)

In the current $Rb_3Ta_5O_{14}$ study, the atomic displacement parameters of all 28 atoms were refined using an anisotropic model. For all Rb atoms, very large mean-squared displacements were observed. This matches similar findings for the Cs atoms in $Cs_3Ta_5O_{14}$. Large displacement parameters have been reported for Rb atoms in a number of other inorganic materials (Desgardin et al., 1977; Okada et al., 1977; Goodenough et al., 1976; Gasperin & le Bihan, 1980; Michel et al., 1980). In general, such displacements should be understandable in terms of the the atomic packing, interpreted in terms of coordination number, bond lengths and bond angles.

The O coordination numbers are 18, 15, 11 and 15 for Rb1, Rb2, Rb3 and Rb4, respectively, with all coordinating Rb—O contacts shorter than 4.25 Å. For Rb1, the shortest two of those contacts are collinear along $a \simeq$ [001] vector and are matched by a correspondingly small U_{33} component. In

Figure 3
An *ATOMS* (Dowty, 1995) polyhedral view of a (205) plane slice through the $Rb_3Ta_5O_{14}$ unit cell showing the pyrochlore-like layering.
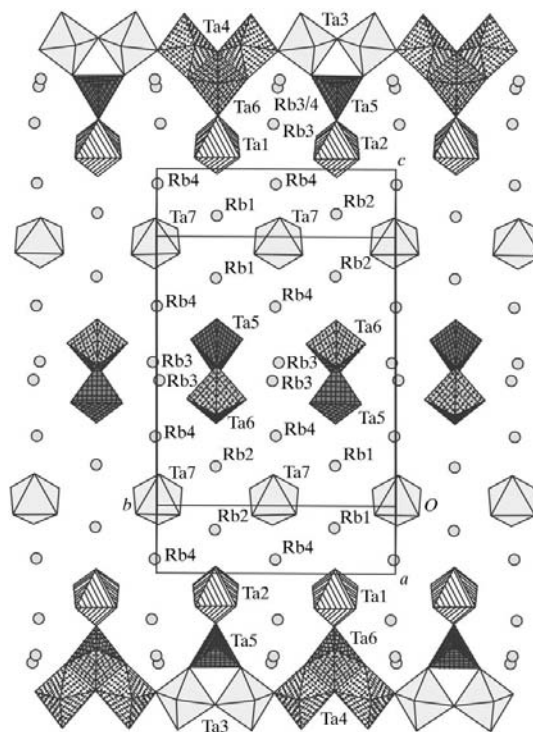

Figure 4
A second (205) plane slice revealing the isolated polyhedral layers by which successive pyrochlore-like layers connect.

contrast, Rb2 has more nearly isotropic vibrational motion, reflecting the more even angular distribution of its contacts. Two Rb3 atoms are located close to the centre of the large cavity. They have one short Rb3—O16 bond and also four short Rb3···Rb contacts in the (010) plane [Rb3···Rb3 3.5097 (18) and 4.1508 (19) Å, and Rb3···Rb4 3.6412 (15) and 3.8795 (18) Å]. These bonds are significantly shorter than the 4.95 Å Rb—Rb bonds in metallic (body centred cubic) Rb (Barrett, 1956). Vibrations orthogonal to that plane are consequently much larger for Rb3. The Rb4 atoms are located near wedge-shaped corners of the large cavity and have very large U_{22} vibrations [0.1057 (11) Å^2]. This is quite understandable because the planes of that 'wedge' are actually planar intercavity interfaces, *i.e.* channels along which the Rb4 atoms have a greater degree of freedom. These channels were shown in Fig. 2(*b*). Rb4 has one very short Rb4—O15 bond to an O atom in the middle of the 'wedge edge' and may undergo some degree of librational motion with respect to that 'edge' axis.

The existence of such short Rb3—Rb3 bonds in this structure, oriented along [100] channels, suggest that some degree of metallic conductivity may occur. If Li could be substituted for Rb, this material may be an ionic conductor.

Experimental

Rb$_3$Ta$_5$O$_{14}$ crystals were grown as a by-product during attempts to form four-layered Rb$_2$Ca$_2$Ta$_4$O$_{13}$ perovskites using a flux technique. Reagent grade chemicals, 5.0 g in total, were comprised of Rb$_2$CO$_3$ (0.2 mmol), CaCO$_3$ (0.4 mmol), Ta$_2$O$_5$ (0.4 mmol) and an RbCl (39 mmol) flux. The dry mixture was placed in a Pt crucible and heated rapidly to 1373 K in a resistance furnace. This maximum temperature was sustained for 10 h, followed thereafter by very slow cooling at 2.8 K h^{-1} to 723 K. Subsequently, the sample was cooled rapidly to room temperature. Transparent rectangular prisms of the Rb$_3$Ta$_5$O$_{14}$ phase described herein grew in conjunction with another, as yet unsolved, hexagonal phase of expected composition Ca$_2$Ta$_2$O$_7$, as determined approximately using X-ray fluorescence. For the particular single crystal used in this experiment, an EDAX (energy dispersive analytical X-ray) analysis showed no measurable Ca content.

Crystal data

Rb$_3$Ta$_5$O$_{14}$
$M_r = 1385.13$
Orthorhombic, *Pnma*
$a = 7.3677$ (3) Å
$b = 14.7904$ (19) Å
$c = 25.379$ (3) Å
$V = 2765.6$ (5) Å^3
$Z = 8$
$D_x = 6.653$ Mg m^{-3}

Synchrotron radiation
$\lambda = 0.8499$ Å
Cell parameters from 10 reflections
$\theta = 21.6$–43.8°
$\mu = 62.9$ mm^{-1}
$T = 298$ K
Prism, colourless
$0.07 \times 0.04 \times 0.04$ mm

Data collection

Tsukuba-BL14*A* diffractometer
$\omega/2\theta$ scans
Absorption correction: analytical (*Xtal*3.7 *ABSORB*; Hall *et al.*, 2000) $T_{min} = 0.093$, $T_{max} = 0.220$
35 705 measured reflections
8727 independent reflections
8498 reflections with $F > 0$

$R_{int} = 0.053$
$\theta_{max} = 50°$
$h = -13 \rightarrow 13$
$k = -26 \rightarrow 26$
$l = 0 \rightarrow 45$
6 standard reflections every 194 reflections intensity decay: none

Table 1
Selected interatomic distances (Å).

Ta1—O3	1.902 (4)	Rb1—O9	4.226 (8)
Ta1—O5	1.909 (7)	Rb1—Rb1^{viii}	4.272 (3)
Ta1—O17	2.003 (4)	Rb1—Rb4	4.3072 (17)
Ta1—O1	2.220 (6)	Rb2—O6	3.016 (7)
Ta2—O4	1.918 (5)	Rb2—O14^v	3.148 (5)
Ta2—O6	1.923 (7)	Rb2—O12	3.242 (5)
Ta2—O17^i	1.992 (4)	Rb2—O12^{ix}	3.325 (5)
Ta2—O2	2.170 (6)	Rb2—O15	3.571 (5)
Ta3—O11	1.860 (5)	Rb2—O10^v	3.595 (7)
Ta3—O13	1.934 (4)	Rb2—O4	3.669 (5)
Ta3—O9	1.9519 (18)	Rb2—O14^{ix}	3.766 (5)
Ta3—O16	1.967 (4)	Rb2—O10^{ix}	3.999 (6)
Ta3—O3	2.020 (5)	Rb2—Rb2^x	4.306 (2)
Ta3—O7^{ii}	2.144 (5)	Rb2—Rb4	4.3595 (17)
Ta4—O16^{iii}	1.871 (4)	Rb3—O16^{iii}	2.679 (5)
Ta4—O12	1.907 (5)	Rb3—O17^{iii}	2.981 (5)
Ta4—O14	1.972 (4)	Rb3—O3^{iii}	3.038 (5)
Ta4—O4	1.997 (5)	Rb3—O8^{ii}	3.147 (5)
Ta4—O10	2.030 (2)	Rb3—O7^{xi}	3.243 (5)
Ta4—O8^{ii}	2.115 (5)	Rb3—O8^{xii}	3.245 (5)
Ta5—O7	1.840 (5)	Rb3—O4	3.325 (5)
Ta5—O5	1.937 (7)	Rb3—O17^i	3.378 (5)
Ta5—O2^{iv}	1.941 (6)	Rb3—Rb3^{xiii}	3.5097 (19)
Ta5—O1^v	2.130 (6)	Rb3—O1	3.5615 (5)
Ta6—O8	1.917 (4)	Rb3—Rb4^{xii}	3.6412 (16)
Ta6—O6	1.928 (7)	Rb3—O7^i	3.768 (5)
Ta6—O1^i	1.971 (6)	Rb3—Rb4	3.8796 (18)
Ta6—O2^v	2.157 (6)	Rb3—O2	3.9110 (15)
Ta6—O10^v	2.168 (6)	Rb3—Rb3^{xii}	4.1508 (19)
Ta7—O15^{vi}	1.932 (5)	Rb3—Rb4^{ii}	5.072 (2)
Ta7—O14^v	1.955 (4)	Rb4—O15	2.736 (5)
Ta7—O15	1.977 (5)	Rb4—O13^{vii}	3.093 (5)
Ta7—O13^{vii}	1.992 (4)	Rb4—O4	3.162 (5)
Ta7—O2^{vi}	2.035 (4)	Rb4—O14^v	3.193 (5)
Ta7—O11^{viii}	2.052 (4)	Rb4—O3^{iii}	3.228 (5)
Ta7—Rb4	3.6385 (13)	Rb4—O7^{iii}	3.267 (5)
Rb1—O9^{viii}	3.126 (7)	Rb4—O8	3.300 (5)
Rb1—O5	3.128 (7)	Rb4—O16^{iii}	3.515 (5)
Rb1—O13^v	3.156 (5)	Rb4—O11^{iii}	3.607 (5)
Rb1—O11^{viii}	3.343 (4)	Rb4—O12	3.723 (5)
Rb1—O9^v	3.377 (8)	Rb4—O5	3.757 (2)
Rb1—O11	3.496 (5)	Rb4—O6	3.829 (2)
Rb1—O3	3.891 (5)	Rb4—O16^{vii}	3.856 (5)
Rb1—O15	3.906 (5)	Rb4—O17^i	3.951 (4)
Rb1—O13^{viii}	3.923 (5)	Rb4—O17^{iii}	3.971 (4)
Rb1—O7	4.134 (5)		

Symmetry codes: (i) $1 - x, \frac{1}{2} + y, -z$; (ii) $1 + x, y, z$; (iii) $x, \frac{1}{2} - y, z$; (iv) $1 - x, y - \frac{1}{2}, -z$; (v) $x - 1, y, z$; (vi) $x - \frac{1}{2}, y, \frac{1}{2} - z$; (vii) $x - 1, \frac{1}{2} - y, z$; (viii) $x - \frac{1}{2}, \frac{1}{2} - y, \frac{1}{2} - z$; (ix) $x - \frac{1}{2}, \frac{3}{2} - y, \frac{1}{2} - z$; (x) $\frac{1}{2} + x, \frac{3}{2} - y, \frac{1}{2} - z$; (xi) $1 + x, \frac{1}{2} - y, z$; (xii) $1 - x, 1 - y, -z$; (xiii) $2 - x, 1 - y, -z$.

Refinement

Refinement on F
$R = 0.043$
$wR = 0.047$
$S = 3.28$
8498 reflections
219 parameters

$(\Delta/\sigma)_{max} = 0.002$
$\Delta\rho_{max} = 7.30$ e Å^{-3}
$\Delta\rho_{min} = -8.47$ e Å^{-3}
Extinction correction: Zachariasen (1967)
Extinction coefficient: 3229 (79)

A small $66 \times 56 \times 19$ μm crystal exhibiting (100), (010) and (001) faces was used for structural analysis. A half sphere of diffraction data to $2\theta = 100°$ was measured at a wavelength of 0.8499 (1) Å, carefully chosen to avoid the 0.81554 Å Rb *K*-absorption edge (Sasaki, 1990). The data were measured using *Diff*14*A Software* (Vaalsta & Hester, 1997) to drive a horizontal-type four-circle Rigaku diffractometer mounted on BL14*A* (Satow & Iitaka, 1989) of the Photon factory synchrotron at Tsukuba. The wavelength was calibrated using a spherically ground standard Si crystal. An eight-channel avalanche photodiode detector was used for photon counting (Kishimoto *et al.*,

inorganic compounds

1998). Six standard reflections were measured every 194 reflections and variation of those standards remained within 0.8% for four of the more intense standards and within 2.5% for the weaker two.

The direct-methods phasing algorithms of the *SHELXS*97 (Sheldrick, 1997) package provided an initial solution assuming $P2_111$ symmetry. This was subsequently refined and transformed to the correct origin using *Xtal*3.7 (Hall *et al.*, 2000), with *PLATON* (Spek, 2001) suggesting the final *Pnma* symmetry adopted here. The measured reflection intensities largely conform with the systematic absences expected of this space group, though of the 2436 measured absences, 273 had $I \geq 3\sigma(I)$, especially those violating the conditions $0kl$: $k+l = 2n$ and $hk0$: $h = 2n$. Inspection of the most intense of those reflections suggested poor equivalence amongst Friedel pairs, which typically differed by more than a factor of two. It is possible that these absence violations are Renninger reflections arising from multiple scattering from other reciprocal lattice points on the Ewald sphere. The high scattering cross-section of Ta in conjunction with the high density of reciprocal lattice points owing to the large *c*-axis parameter in real space, serve to enhance the likelihood of such scattering processes. On the other hand, the atomic displacement parameters, as well as the charge density, as detailed below, suggest that some small structural cause may exist, lowering the symmetry.

The merging *R* factor reduced from 5.9 to 5.3% after applying an analytical absorption correction (de Meulenaer & Tompa, 1965). Dispersion and absorption coefficients were determined from the tables of Sasaki (1989, 1990) and the final weighted least-squares *R* factor reduced to $wR(F) = 0.046$.

The final $\Delta\rho$ difference maps indicate a maximum peak of 7.4 e $\mathring{A}^{-3}$ very close to the Rb1 atom core, with all other peaks ≤ 4.7 e $\mathring{A}^{-3}$. The largest magnitude electron depletion of -9.2 e $\mathring{A}^{-3}$ is also located diametrically across the Rb1 nucleus, giving the appearance of a strong dipole across this atom. Omitting the Rb1 atom from a structure-factor calculation reveals a rounded triangular region of electron density, with two vertices symmetric across the mirror plane. This suggests that either the mirror plane is only a pseudo-mirror or Rb1 may be statically disordered, dynamically disordered or a mixture of both. Similar $\Delta\rho$ topography is observed around Rb2, also on the mirror plane, but the maximum and minimum values are around one-quarter the values for Rb1. Minor evidence of other potential mirror-plane irregularities comes from Ta1, Ta2, Ta5, Ta6, O1, O2, O5 and O6, which all have *m* symmetry in conjunction with slightly larger U_{22} vibrational components. On the other hand, O9 and O10 also have *m* symmetry but do not exhibit such tendencies.

To test if the mirror symmetry was really broken by the Rb1 atom site, the structure was refined in three lower-symmetry subgroups of *Pnma*. The $\Delta\rho$ topography localized around the Rb1 atom persisted in $Pn2_1a$, $P2_1/n11$ and $P112_1/a$, albeit with slightly different maximum and minimum magnitudes. *R* factors for the three lower-symmetry solutions were $wR(F) = 0.042$, 0.045 and 0.049, respectively. This common topography suggests that the *Pnma* symmetry adopted here is appropriate and either the Rb1 atom is vibrating anharmonically or it is disordered across three positions (two related by *m* symmetry). A refinement of two disordered Rb1 atom sites was attempted in the

Pnma space group and this reduced $wR(F)$ from 0.0462 to 0.0458. Purely for conciseness though, only the simplest structural form was adopted herein.

Additional strong $\Delta\rho$ depletions of ≥ -7.8 e$\mathring{A}^{-3}$ are located around several of the Ta atoms. Given the large atomic number of Ta atoms and their typically deformed octahedral environments, such large residual charge densities are not unexpected.

Data collection: *Diff*14*A Software* (Vaalsta & Hester, 1997); cell refinement: *Xtal*3.7 (Hall *et al.*, 2000); data reduction: *Xtal*3.7; program(s) used to solve structure: *SHELXS*97 (Sheldrick, 1997); program(s) used to refine structure: *Xtal*3.7; molecular graphics: *ATOMS* (Dowty, 1995) and *Xtal*3.7; software used to prepare material for publication: *Xtal*3.7.

References

Barrett, C. S. (1956). *Acta Cryst.* **9**, 671–677.
Desgardin, G., Robert, C., Groult, D. & Raveau, B. (1977). *J. Solid State Chem.* **22**, 101–111.
Dowty, E. (1995). *ATOMS*. Version 5.1. Shape Software, Kingsport, Tennessee 37663, USA.
Gasperin, M. & le Bihan, M. T. (1980). *J. Solid State Chem.* **33**, 83–89.
Goodenough, J. B., Hong, H. Y. P. & Kafalas, J. A. (1976). *Mater. Res. Bull.* **11**, 203–220.
Hall, S. R., du Boulay, D. J. & Olthof-Hazekamp, R. (2000). Editors. *Xtal*3.7. University of Western Australia, Australia. Web address: http://Xtal.crystal.uwa.edu.au/.
Johnson, C. K. (1970). *ORTEP*. Report ORNL-3794, 2nd revision. Oak Ridge National Laboratory, Tennessee, USA.
Kihlborg, L. & Hussain, A. (1979). *Mater. Res. Bull.* **14**, 667–674.
Kishimoto, S., Ishizawa, N. & Vaalsta, T. P. (1998). *Rev. Sci. Instrum.* **69**, 384–391.
Lukaszewicz, K., Pietraszko, A., Stepian-Damm, J. & Kolpakova, N. N. (1994). *Mater. Res. Bull.* **29**, 987–992.
Meulenaer, J. de & Tompa, H. (1965). *Acta Cryst.* **19**, 1014–1018.
Michel, C., Guyomarch, A. & Raveau, B. (1980). *J. Solid State Chem.* **34**, 193–198.
Okada, K., Marumo, F. & Iwai, S. I. (1977). *Acta Cryst.* B**33**, 3345–3349.
Sasaki, S. (1989). KEK Report 88-14. National Laboratory for High Energy Physics, Tsukuba 5–24, Japan.
Sasaki, S. (1990). KEK Report 90-16. National Laboratory for High Energy Physics, Tsukuba 7–26, Japan.
Satow, Y. & Iitaka, Y. (1989). *Rev. Sci. Instrum.* **60**, 2390–2393.
Serafin, V. M. & Hoppe, R. (1982). *Z. Anorg. Allg. Chem.* **493**, 77–92.
Sheldrick, G. M. (1997). *SHELXS*97. University of Göttingen, Germany.
Spek, A. L. (2001). *PLATON*. Utrecht University, The Netherlands.
Vaalsta, T. P. & Hester, J. R. (1997). *Diff*14*A Software*. Photon Factory, Tsukuba, Japan.
Zachariasen, W. H. (1967). *Acta Cryst.* **23**, 558–564.